chemengineering

MDPI

Article

Comparative Study of Physicochemical Characteristics and Catalytic Activity of Copper Oxide over Synthetic Silicon Oxide and Silicon Oxide from Rice Husk in Non-Oxidative Dehydrogenation of Ethanol

Manshuk Mambetova [1], Gaukhar Yergaziyeva [1,2,*], Kusman Dossumov [1], Kydyr Askaruly [3], Seitkhan Azat [3], Kalampyr Bexeitova [2], Moldir Anissova [1] and Bedelzhan Baizhomartov [1]

[1] Center of Physical and Chemical Methods of Research and Analysis, Almaty 050012, Kazakhstan
[2] Faculty of Chemistry and Chemical Technology, Al-Farabi Kazakh National University, Almaty 050040, Kazakhstan
[3] Laboratory of Engineering Profile, Satbayev University, Almaty 050013, Kazakhstan
* Correspondence: ergazieva_g@mail.ru

Abstract: The article presents the results of comparative research on the physicochemical characteristics and catalytic activity of copper oxide supported on synthetic SiO_2 and SiO_2 (RH) from rice husk. SiO_2 (RH) is more hydrophobic compared to SiO_2, which leads to the concentration of copper oxide on its surface in the form of a "crust", which is very important in the synthesis of low-percentage catalysts. According to SEM, XRD, and TPR-H_2, the use of SiO_2 (RH) as a carrier leads to an increase in the dispersion of copper oxide particles, which is the active center of ethanol dehydrogenation.

Keywords: non-oxidative dehydrogenation; ethanol; rice husk; silicon oxide; copper oxide; catalyst

Citation: Mambetova, M.; Yergaziyeva, G.; Dossumov, K.; Askaruly, K.; Azat, S.; Bexeitova, K.; Anissova, M.; Baizhomartov, B. Comparative Study of Physicochemical Characteristics and Catalytic Activity of Copper Oxide over Synthetic Silicon Oxide and Silicon Oxide from Rice Husk in Non-Oxidative Dehydrogenation of Ethanol. *ChemEngineering* **2022**, *6*, 74. https://doi.org/10.3390/chemengineering6050074

Academic Editor: Dmitry Yu. Murzin

Received: 15 August 2022
Accepted: 19 September 2022
Published: 28 September 2022

1. Introduction

Acetaldehyde is one of the most important chemicals. It can be used as a raw material for the production of acetic acid, butanol, 1,3-butylene glycol, acetic anhydride, ethyl acetate, butylaldehyde, crotonaldehyde, pyridine, and many other products [1–3]. In addition, it is widely used in industries, including the food industry, the plastic industry, as well as in the pharmaceutical and cosmetic industries in the production of materials [4–6].

The main industrial method for producing acetaldehyde is the oxidation of valuable ethylene in the presence of aqueous solutions of expensive palladium and copper chloride. This technology is characterized by the formation of a number of toxic organochlorine by-products, including acetic acid and croton aldehyde, dissolved in large amounts of water. Recently, against the background of tightening requirements for environmentally friendly technologies and the desire to shift away from oil dependence, interest in the synthesis of acetaldehyde by ethanol dehydrogenation has again increased [7].

Ethanol is very attractive due to its availability and safety during storage and handling [8,9]. In addition, ethanol is relatively inexpensive, it is easy to transport, it has low toxicity, and it does not contain catalytic poisons such as sulfur, chlorine, etc. More importantly, ethanol can be produced from renewable raw materials by the fermentation of biomass, as well as from agro-industrial waste, residues of timber, and the organic fraction of municipal solid waste. Ethanol thus produced is called bioethanol, which is a mixture of ethanol and water with a molar ratio of 1:13 (about 12 wt.% ethanol) [10,11]. It should be noted that since biomass absorbs carbon dioxide from the atmosphere for its growth, the processing of ethanol obtained from biomass does not contribute to global warming. Two gas-phase processes of ethanol conversion to acetaldehyde are known [12,13]: selective catalytic oxidation with oxygen or air and non-oxidative catalytic dehydrogenation. The non-oxidative dehydrogenation of ethanol to acetaldehyde in comparison with the

oxidative dehydrogenation method has obvious advantages such as no oxidant, its partial oxidation to acetic acid and carbon dioxide, and that the resulting acetaldehyde is easily separated from the reaction by-products. In addition, the non-oxidative dehydrogenation of ethanol is inherently safe, while the mixture of ethanol and oxygen presents a serious problem due to the explosive nature of large-scale industrial processes [2,14]. To create a competitive technology for the production of acetaldehyde from ethanol, it is necessary to develop an efficient catalyst. The activity and selectivity of catalysts depend on the physical and chemical characteristics of the active components. As a general rule, catalysts for the dehydrogenation of alcohol to acetaldehyde can be mainly divided into two types: metal (Cu, Ag, Pd, Au, etc.) and metal oxides (CuO, ZnO, MgO, Cr_2O_3, etc.) [15–25]. Among these catalysts, copper-based catalysts are very active and highly selective against acetaldehyde, partly because Cu can split C–C and C–O bonds at much lower speeds than other transition metals (Pd and Pt) [26]. However, the main problem of copper catalysts is their rapid deactivation. Therefore, special attention is paid to preventing copper sintering and extending the life of the catalyst. Bueno et al. [27] found that the selectivity to acetaldehyde in ethanol dehydrogenation is related to the dispersion of copper. Cassinelli and co-workers [28,29] reported that Cu^+ cations are more active in ethanol dehydrogenation, while other groups of authors [29] found that Cu metal particles are responsible for the activity of ethanol dehydrogenation. The catalytic activity and stability of the catalyst in ethanol dehydrogenation also depend on the nature of the support. A good carrier should provide the necessary dispersion of the active phase (Cu), possibly stabilizing it during the high-temperature reaction [30]. As a carrier for copper, the following have been studied: silicon oxide (SiO_2) [31,32] mesoporous carbon [33], silicon carbide (SiC) [34], coated with a carbon layer of SiO_2 [35], etc.

In our work, synthetic (commercial) silicon oxide (SiO_2) and silicon oxide synthesized from rice husk (SiO_2 (RH)) were examined as a carrier for copper oxide. Rice husks are a cheap, predominant by-product in the process of grinding uncooked grains of rice in agriculture [36]. Usually, it is burned or thrown away, which leads not only to the depletion of resources but also to environmental pollution. RH has great potential to develop various ceramic materials such as refractories, glass, household appliances, oxide, and non-oxide ceramics, silicate airgel, and other composites [37].

The authors [38,39] note that rice husks are used as a binder and additive to concrete in construction, in the production of animal feed and fertilizer, as well as in the production of biofuels. Rice husks are also used to produce silica [40]. In addition, many studies have analyzed the application of RH to wastewater treatment.

Comparative studies have been carried out on the influence of the nature of silicon oxide on the activity and selectivity of copper oxide in the process of obtaining acetaldehyde by non-oxidative dehydrogenation of ethanol. The physicochemical characteristics of the developed catalysts were analyzed by the methods of XRD, SEM, TGA, FTIR, TPR-H_2, and TPD-ammonia.

2. Materials and Methods

2.1. Reagents and Materials

Chemicals such as copper nitrate ($Cu(NO_3)_2 \cdot 6H_2O$; T4163-68), synthetic silicon oxide (SiO_2 carrier), technical ethanol 95%, (Talgar alcohol LLP), Argon (Ar) (IhsanTechnogaz LLP), and Helium (He) (IhsanTechnogaz LLP) were used as starting materials.

2.2. Synthesis of Catalysts

A detailed procedure for obtaining silicon dioxide SiO_2 (RH) from rice husks is described in [41]. Catalysts supported on synthetic silicon oxide (3–5 wt.% CuO/SiO_2) were prepared by the capillary impregnation of silicon oxide SiO_2 according to its moisture capacity with an aqueous solution of copper nitrate salt ($Cu(NO_3)_2 \cdot 6\ H_2O$, 99%, T4163-68, Minsk, Belarus). Catalysts on silicon oxide from rice husk (3–5 wt.% CuO/SiO_2 (RH)) were also prepared by the capillary impregnation of silicon oxide (RH) according to its moisture

capacity with an aqueous solution of copper nitrate salt ($Cu(NO_3)_2 \cdot 6H_2O$, 99%, T4163-68, Minsk, Belarus). After that, the catalysts were dried at 150 °C for two hours and calcined at 350 °C for three hours in a stream of air at atmospheric pressure.

2.3. Characterization

The carriers and catalysts were characterized by a complex of modern physicochemical methods. The morphology of the samples was studied using a low-vacuum scanning electron microscope complete with energy-dispersive X-ray microanalysis system (JSM-6490 LA, Jeol, Tokyo, Japan). The main electron beam is generated by a heated tungsten filament or field ejection gun and is typically accelerated by applying a voltage of 1–30 kV. The presence of electromagnetic lenses leads to the focusing of the beam on the sample to a spot size in the nanometer range. The study of the surface morphology of the obtained samples was carried out by analyzing the data of the secondary electron detector.

The phase composition and crystal structure of the obtained samples were studied with an X-ray diffractometer (XRD, X′ Pert Pro MPD, Malvern Panalytical, Almelo, Netherlands) with Cu-Kα radiation (α = 0.154 nm).

The reducibility of the prepared catalyst was studied using the method of temperature-programmed hydrogen reduction (TPR-H_2) on a chemisorption analyzer (UNISIT, USGA-101, Moscow, Russia). The setup consists of a gas treatment system, a tube furnace flow reactor (internal diameter 4 mm), and a thermal conductivity detector. The samples (0.063 g) were firstly pretreated by Ar at 400 °C for 40 min, then cooled down to room temperature, and followed by turning the flow of 5 vol.% H_2 and 95 vol.% Ar into the system with a flow rate of 30 mL/min. The samples were heated from room temperature to 950 °C at a rate of 10 °C/min. The change in the hydrogen concentration was monitored using a thermal conductivity detector.

The temperature-programmed desorption of ammonia (TPD-NH_3) was carried out on the a chemisorption analyzer (UNISIT, USGA-101, Moscow, Russia). Ammonia (NH_3) was used as probe molecules to determine the acidity of catalysts. To carry out the analysis, the sample was previously saturated with the analyzed substance, the weakly bound molecules were blown off, then linear heating was started in the inert gas current. At a certain temperature, which depends on the force of the interaction between the probe molecule and the active center, the substance is desorbed from the composite material. To carry out TPD-ammonia, the sample (0.06 g) was first treated (pretreatment), i.e., heated at a temperature of 500 °C, holding for 40 min in a helium flow (25 mL/min), cooling to a temperature of 60 °C, saturation with ammonia at this temperature for 15 min, then blowing weakly bound ammonia in a helium flow at 100 °C and cooling to 60 °C. In the second stage, the temperature was raised from 5 °C/min to 800 °C in the helium of 30 mL/min. Then, a trap was used in case of water release from the sample; further, there was cooling in the furnace up to 100 °C.

Thermogravimetric analysis and differential thermal analysis (TGA and TG-DTA) was carried out on a simultaneous thermal analyzer (NETZSCH STA 409 PC/PG, 6000 device, Perkin Elmer, Inc., Waltham, MA, USA) in a nitrogen atmosphere. The temperature range of the study ranged from 50 to 950 °C with a heating rate of 10 °C/min^{-1}.

The FTIR spectrometer (Bruker Optik GmbH, VERTEX 70, Ettlingen, Germany) was used to explore functional groups of molecules and compounds. The FTIR spectra were recorded using a VERTEX 70 equipped with a PIKE MIRacle ATR single-disturbed internal total reflection prefix with a germanium crystal in the range of 4000–500 cm^{-1}. The results were processed according to the OPUS 7.2.139.1294 program.

2.4. Testing of Catalysts in Ethanol Conversion

Tests of the activity of carriers and catalysts in the non-oxidative dehydrogenation of ethanol were carried out on an automated flow-through catalytic setup. The installation includes a gas flow regulator, a liquid pump, a reactor, an evaporator, a switch, and a separator (Figure 1).

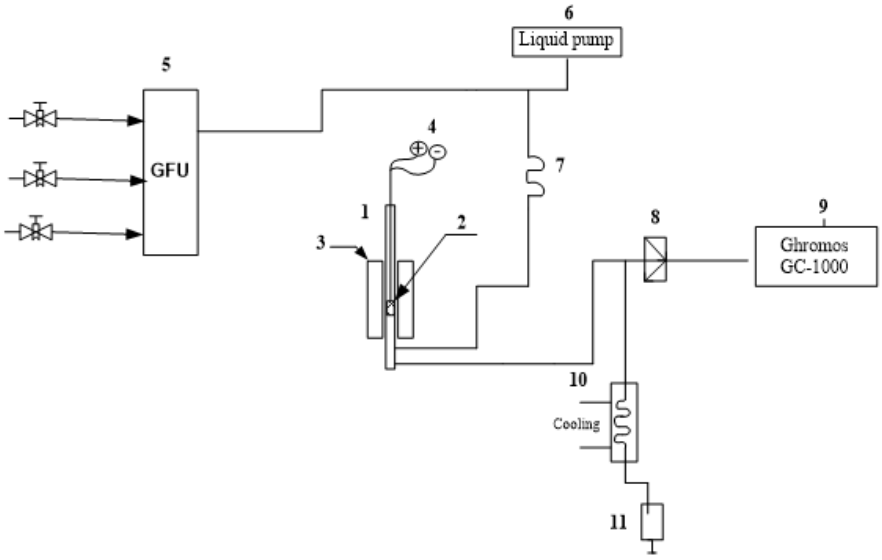

Figure 1. Flow-through catalytic setup of high pressure. 1—reactor; 2—catalyst; 3—furnace; 4—reactor thermocouple; 5—gas flow regulator; 6—liquid pump; 7—evaporator; 8—commutator; 9—analysis on the GC-1000 chromatograph; 10—separator; 11—collection of liquid fractions.

The stainless steel reactor was located vertically. The flow from the evaporator was fed upwards and passed through the container and the reactor pipe (length 335 mm, diameter 12.5 mm) containing the catalyst. Gases from the reactor's outlet entered the separator, where part of the flow was channeled through the metering valve and the heated line into the chromatograph for analysis. Catalytic tests were carried out with a space velocity (WHSV) in the range of 0.5–1.5 h^{-1} and a temperature range of 150–400 °C. The ethanol flow rate was 0.02 mL/min and the experiments were carried out without inert gas. Ethanol conversion and product selectivity were calculated according to the equations:

$$\text{Ethanol conversion (mol.\%)} = \frac{[\text{Ethanol}]\text{inlet} - [\text{Ethanol}]\text{outlet}}{[\text{Ethanol}]\text{inlet}} \times 100\% \quad (1)$$

$$\text{Acetaldehyde selectivity (mol.\%)} = \frac{[\text{Acetaldehyde}]\text{outlet}}{[\text{Ethanol}]\text{inlet} - [\text{Ethanol}]\text{outlet}} \times 100\% \quad (2)$$

2.5. Analysis of Reaction Products

The reaction products were identified on "CHROMOS GC-1000" using absolute calibration and thermal conductivity detectors. The reaction products H_2, N_2, and O_2 were determined using a column with a sorbent CaA, column length l = 2 m, column diameter d = 3 mm, and T = 350 °C. To determine CO, CO_2, and CH_4 used a column with the HP/Plot Q speed of the carrier gas (H_2)—20 mL/min, temperature column—T = 250 °C. For the determination of ethanol, acetaldehyde, dietoxyethane, etc., a capillary column with an XSEP sorbent was used. The length of the column is 25 m, and the diameter of the column is d = 0.32 mm. The maximum operating temperature is 250 °C.

3. Results

3.1. Characterization

The structures of SiO_2 and SiO_2 (RH) molecules were studied by FTIR spectroscopy. Figure 2a shows the FTIR spectra for fresh SiO_2 and SiO_2 (RH) samples in the range of 750–4500 cm^{-1}. In the spectrum of SiO_2, absorption bands are observed at 794 cm^{-1}, 1049 cm^{-1}, and in the intervals, 2700–3620 cm^{-1} and 1500–1790 cm^{-1}. Absorption bands at 794 cm^{-1} and 1049 cm^{-1} are typical for silicon oxide; the absorption bands are associated with the vibration of the Si–O bond and the asymmetric valence vibration of the siloxane bonds (Si-O-Si), respectively. The broad absorption band in the range of 2700–3620 cm^{-1}

refers to the valency vibrations of the water molecule. Absorption bands were in the range of 1500–1790 cm^{-1} to deformation vibrations of the water molecule [42]. The absorption bands 795 and 1049 cm^{-1}, characteristic of silicon oxide, are also observed on the SiO_2 (RH) sample, indicating the presence of a Si–O and Si–O–Si bond [43]. The SiO_2 (RH) sample also exhibits absorption bands characteristic of silicon oxide at 795 and 1049 cm^{-1}, indicating the presence of Si–O and Si–O–Si bonds [43]. The FTIR spectrum SiO_2 (RH) does not have an absorption band of the valence and deformation molecules of the water, which may indicate the hydrophobicity of SiO_2 (RH) compared to SiO_2.

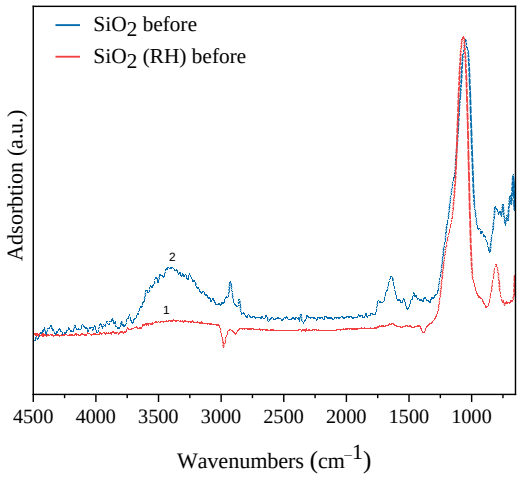

(**a**)

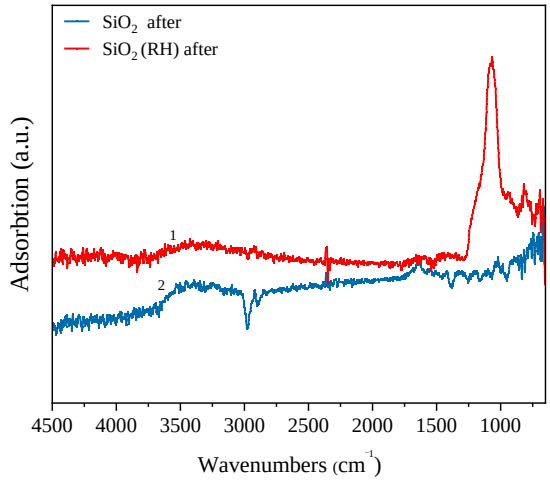

(**b**)

Figure 2. FTIR spectra of samples (**a**) fresh samples, (**b**) samples after the reaction. (1) SiO_2 (RH); (2) SiO_2.

Figure 2b shows the FTIR spectra of SiO_2 and SiO_2 (RH) after testing them in the non-oxidative dehydrogenation of ethanol. It is seen from the figure that SiO_2 (RH) retains the absorption bands characteristic of the Si–O and Si–O–Si bonds, and a new absorption band appears at 900 cm^{-1}, which can be attributed to the Si–O–C bond [44]. In addition, a broad peak appears in the region of 3200–3700 cm^{-1}, which is associated with the O–H valence vibration of the alcohol bond.

After testing SiO_2 in the non-oxidative dehydrogenation of ethanol, the bonds characteristic of silicon oxide are not observed on the FTIR spectrum, which may indicate the destruction of the structure of silicon oxide under the influence of temperature, as well as ethanol and its decomposition products.

Morphological properties of carriers and catalysts were studied by scanning electron microscopy. Micrographs of carriers and catalysts are shown in Figure 3. Figure 3a,b shows that synthetic SiO_2 and silicon oxide obtained from rice husks differ greatly in morphology.

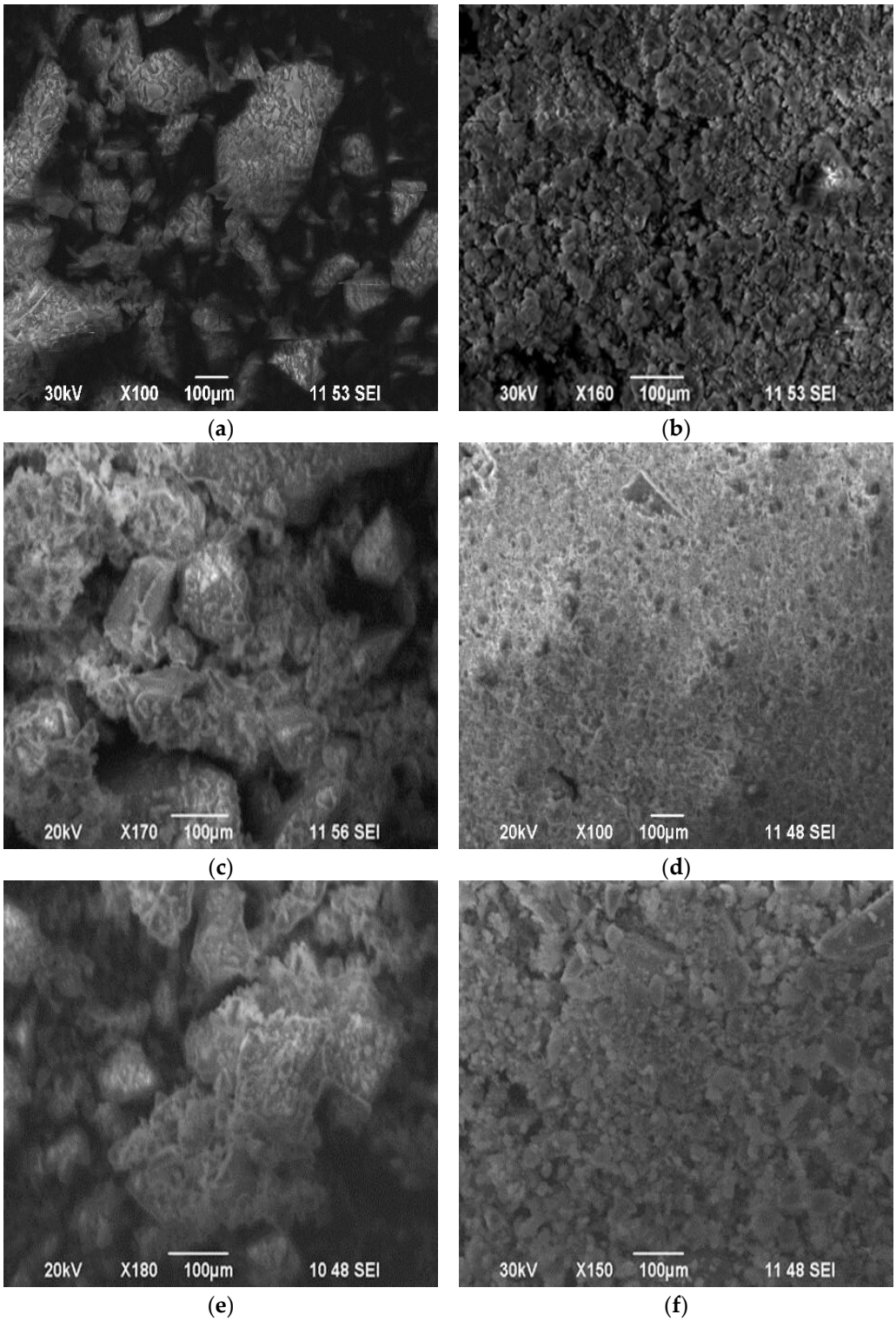

Figure 3. SEM images of fresh samples. (**a**) SiO_2; (**b**) SiO_2 (RH); (**c**) 3 wt.% CuO/SiO_2; (**d**) 3 wt.% CuO/SiO_2 (RH); (**e**) 5 wt.% CuO/SiO_2; (**f**) 5 wt.% CuO/SiO_2 (RH).

The morphology of SiO_2 (RH) is more dispersed compared to SiO_2. The SiO_2 sample consists of aggregates of different shapes and sizes. The support of 3 wt.% copper oxide

to the carrier leads to an increase in the dispersion of particles, compared with 5 wt.% CuO, as in the case of SiO_2 (RH) and SiO_2. On the surface of 3 wt.% CuO/SiO_2 (RH), more amorphous copper oxide particles are observed (Figure 3c), which are distributed more evenly, compared with 5 wt.% CuO/SiO_2 (RH).

Consequently, an increase in the content of copper oxide on a CuO/SiO_2 (RH) sample (up to 5 wt.%) leads to poor dispersion due to volume agglomeration of CuO [45]. Figure 4 shows X-ray diffraction patterns of the fresh catalysts and carriers. The SiO_2 (RH) and SiO_2 carriers have a wide peak at 2θ = 22, which refers to the silicon oxide phase [46–48]. The X-ray diffraction patterns of 3 wt.% CuO/SiO_2 (RH) and 5 wt.% CuO/SiO_2 (RH) catalysts showed diffraction peaks, indicating the formation of relatively small crystalline CuO particles (2θ = 35, 38) [49,50]. For samples of 3 wt.% CuO/SiO_2 and 5 wt.% CuO/SiO_2, there were no clear peaks of copper oxide, despite the fact that copper catalysts based on SiO_2 and SiO_2 (RH) were prepared by the capillary impregnation of the carrier according to its moisture capacity. Probably, detected by us with the FTIR method, the high hydrophilicity of SiO_2 compared with SiO_2 (RH) affected the distribution of copper oxide over the entire volume of the SiO_2 carrier. Therefore, the XRD profiles of 3 wt.% CuO/SiO_2 and 5 wt.% CuO/SiO_2 were not found to have clear peaks related to copper oxide [51]. Due to the hydrophobicity of SiO_2 (RH), copper oxide concentrated on the surface of the carrier in the form of «crust» [52,53], therefore on the XRD profiles of 3 wt.% CuO/SiO_2 (RH) and 5 wt.% CuO/SiO_2 (RH), catalysts show diffraction peaks of CuO particles (2θ = 35, 38). The different hydrophilicity and hydrophobicity of SiO_2 (RH) and SiO_2 silicon oxides led to different distributions of copper oxide on these carriers.

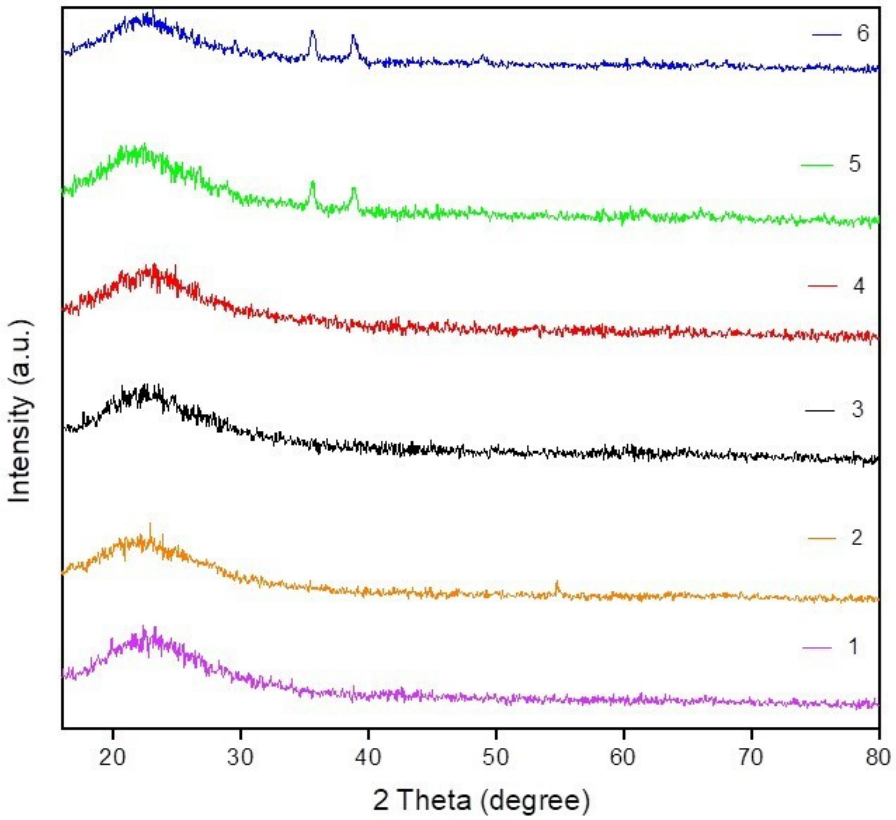

Figure 4. XRD diffractograms of the samples. (1) SiO_2; (2) SiO_2 (RH); (3) 3 wt.% CuO/SiO_2; (4) 5 wt.% CuO/SiO_2; (5) 3 wt.% CuO/SiO_2 (RH); (6) 5 wt.% CuO/SiO_2 (RH).

Thermogravimetric analysis and differential thermal analysis (TGA and TG-DTA) of SiO_2 (RH) and SiO_2 are shown in Figure 5a. Temperature heating for silicon oxides and catalysts ranges from room temperature to 800 °C at 10 °C/min. The weight loss of SiO_2 (RH) at a peak temperature of 69.7 °C is 5.2%, which is due to physically adsorbed water

and CO_2. The SiO_2 sample also has a gradual mass loss at a peak temperature of 96.3 °C, which is 8.5%. These data may be indicative of the hydrophobicity of SiO_2 (RH) and the hydrophilicity of SiO_2 relative to each other [54].

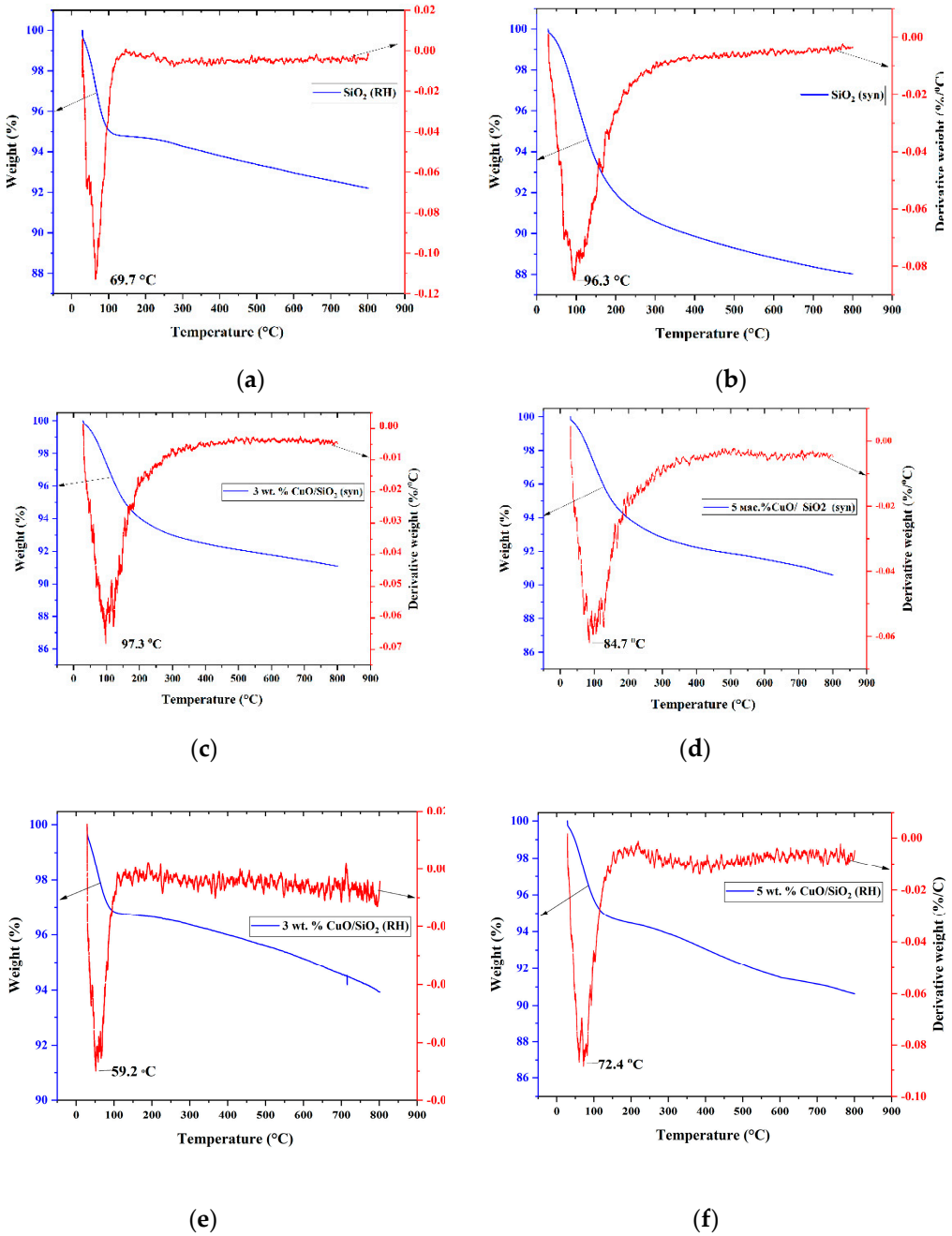

Figure 5. Derivatogram of samples: (**a**) SiO_2 (RH); (**b**) SiO_2; (**c**) 3 wt.% CuO/SiO_2; (**d**) 5 wt.% CuO/SiO_2; (**e**) 3 wt.% CuO/SiO_2 (RH); (**f**) 5 wt.% CuO/SiO_2 (RH).

For catalysts on synthetic media of 3 wt.% CuO/SiO_2 and 5 wt.% CuO/SiO_2, the mass loss line has the same character; the mass loss up to 200 °C is 6.6 and 6.7%, respectively. The weight loss of samples 3 wt.% CuO/SiO_2 (RH) and 5 wt.% CuO/SiO_2 (RH) are 3.4 and 5.6%, respectively. The temperature peaks of the weight loss of the samples are in the range of 60–105 °C; this interval is associated with the loss of physically adsorbed water and CO_2.

The reduction characteristics of the samples were investigated by the TPR-H_2 method. Figures 6 and 7 show the TPR-H_2 curves for all samples. The TPR profiles of SiO_2 and SiO_2 (RH) did not show a clear H_2 absorption signal. On the TPR profile of the catalyst

(Figure 6) 3 wt.% CuO/SiO_2, two peaks are observed with maxima T^1_{max} = 314 °C and T^2_{max} = 475 °C, the amount of adsorbed hydrogen is A^1 = 130 µmol/g and A^2 = 22 µmol/g. It is known [45] that pure copper oxide not supported on the carrier is reduced at a temperature of 250–260 °C. However, depending on the nature of the carrier and the state of the supported copper oxide, the catalyst reduction temperature can be shifted both to the high-temperature and to the low-temperature region. For a catalyst of 5 wt.% CuO/SiO_2, two peaks are observed on the TPR-H_2 curves with maxima of hydrogen absorption temperatures T^1_{max} = 255 °C, A^1 = 269 µmol/g, T^2_{max} = 344 °C, and A^2 = 152 µmol/g [55]. The existence of two peaks in the TPR profile of 5 wt.% CuO/SiO_2 is associated with the reduction in copper oxide with different dispersity. The first peak can be attributed to the reduction in a highly dispersed CuO nanocluster; the second peak refers to the reduction in crystalline CuO. Similar data were obtained in [56,57].

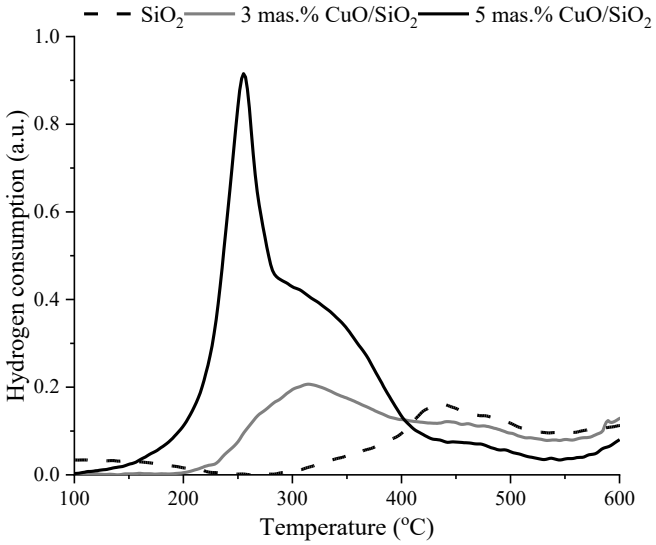

Figure 6. TPR-H_2 profiles of fresh SiO_2 and 3 wt.% CuO/SiO_2, 5 wt.% CuO/SiO_2 catalysts.

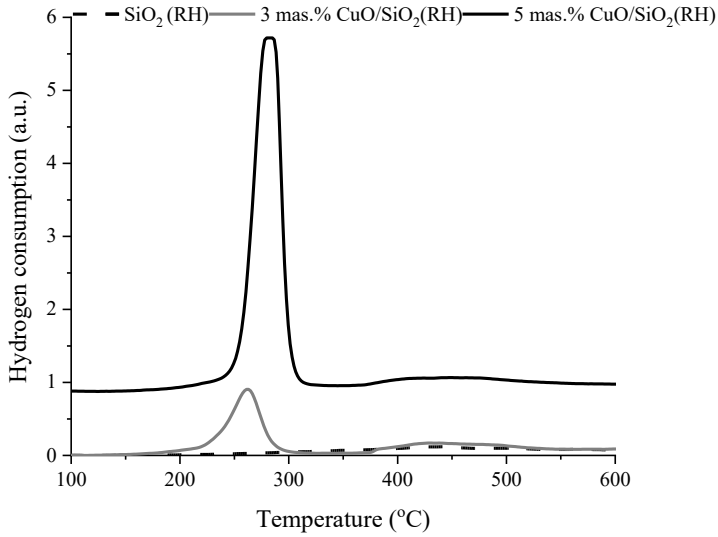

Figure 7. TPR-H_2 profiles of fresh SiO_2 (RH) and 3 wt.% CuO/SiO_2 (RH) and 5 wt.% CuO/SiO_2 (RH) catalysts.

The TPR profile (Figure 7) of a 3 wt.% CuO/SiO_2 (RH) sample presents two peaks of different intensity at T^1_{max} = 263 °C, A^1 = 198 µmol/g and T^2_{max} = 433 °C, A^2 = 75 µmol/g. The support of 3 wt.% of copper oxide on a SiO_2 (RH) carrier leads to an increase in intensity,

and also a decrease in the reduction temperature of the peak related to dispersed copper oxide from 314 to 263 °C and the peak related to the reduction in crystalline CuO from 475 to 433 °C. Increasing the copper oxide content to 5 wt.% leads to a change in the TPR profile of the catalyst. On the TPR profile of the sample 5 wt.% CuO/SiO_2 (RH) is present an intense peak of T^1_{max} = 283 °C, A^1 = 863 μmol/g. With an increase in the content of copper oxide from 3 to 5 wt.%, the T^1_{max} increases from 263 to 283 °C, which is associated with the consolidation of copper oxide particles. It is known [58] that a decrease in the reduction temperature of copper oxide indicates an increase in the dispersion of its particles.

The acid characteristics of the samples were studied by the TPD-ammonia method (Figures 8 and 9, Table 1). According to the literature [12,59], the ammonia desorption peak at low temperatures (100–200 °C) refers to weak acid sites, the desorption peak at moderate temperatures (200–400 °C) corresponds to medium acid sites, and the desorption peak at high temperatures (>400 °C) corresponds to strong acid sites. It follows from the analysis of the obtained profiles of the samples (SiO_2 (RH), 3 wt.% CuO/SiO_2 (RH), 5 wt.% CuO/SiO_2 (RH)) (Figure 8) that SiO_2 (RH) has several weak intensity peaks. Peaks with maxima T^1_{max} = 105 °C and T^2_{max} = 168 °C in the range of 100–170 °C are associated with the presence of weak acid sites. The peak with a maximum at T^3_{max} = 348 °C refers to acid sites with medium strength. The presence of peaks above 400 °C, with maxima at 438, 672, and 734 °C, refers to strong acid centers. A quantitative comparison of the desorbed ammonia shows that medium acid sites prevailed in the composition of SiO_2 (RH). The support of copper oxide to the SiO_2 (RH) carrier leads to an increase in the concentration of weak and medium acid sites. At the same time, the number of weak acid sites is significantly higher by 5 wt.% CuO/SiO_2 (RH) compared to 3 wt.% CuO/SiO_2 (RH).

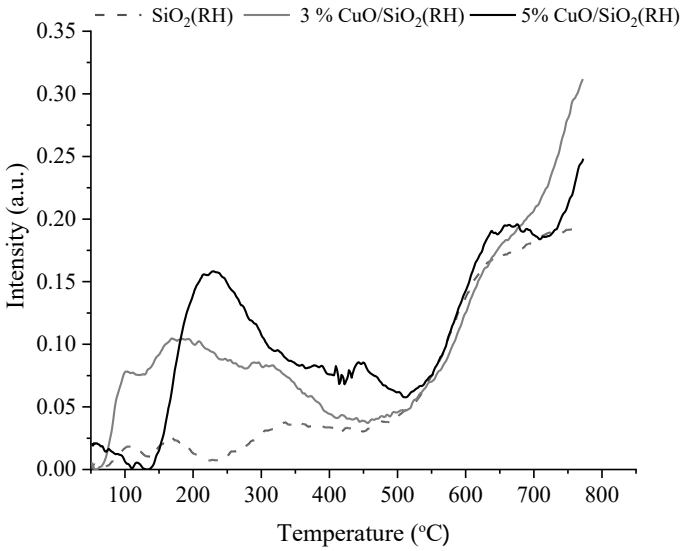

Figure 8. TPD profiles of fresh SiO_2 (RH) and 3 wt.% CuO/SiO_2 (RH) and 5wt.% CuO/SiO_2 (RH) catalysts.

On the TPD profile of samples of SiO_2, 3 wt.% CuO/SiO_2, and 5 wt.% CuO/SiO_2, intense peaks are observed in the region of 100–450 °C and weak intensity peaks in the region of 500–750 °C. Two peaks with maxima at 214 °C and 632 °C are observed on synthetic SiO_2, which confirms the presence of weak and strong acid sites. With the support of copper oxide on silicon oxide and with an increase in the content of copper oxide, the total acidity of the samples increases both in the case of catalysts on SiO_2 and on SiO_2 (RH) (Table 1).

It follows from the results of TPD-ammonia (Table 1) that synthetic silicon oxide and catalysts based on it have weak and strong acid sites. The total acidity of the samples increases from 482 to 968 μmol/g with the support of copper oxide on the carrier and an increase in its concentration on the carrier. In contrast to synthetic silicon oxide and

catalysts based on it, the carrier obtained from rice husks and the catalysts supported on it have additionally medium acid sites. As can be seen from Table 1, the highest concentration of average acid sites of 34 μmol/g is observed on a sample of 3 wt.% CuO/SiO_2 (RH). The total acidity of the samples increases from 78 to 161 μmol/g also with the support of copper oxide to the carrier and an increase in its concentration.

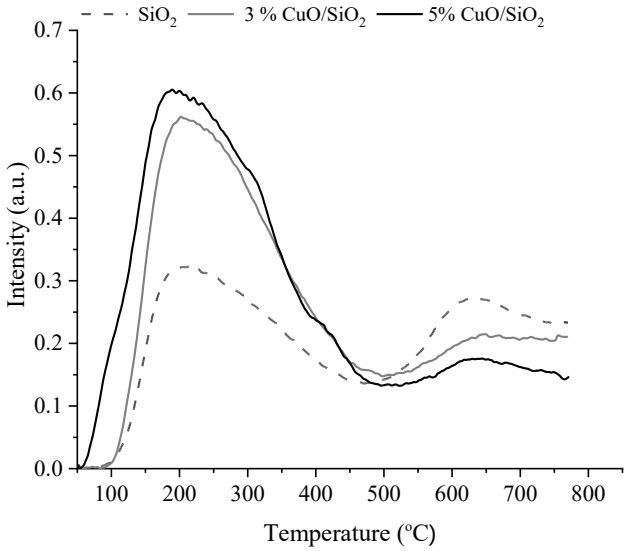

Figure 9. TPD profiles of fresh SiO_2 and 3 wt.% CuO/SiO_2 and 5 wt.% CuO/SiO_2 catalysts.

Table 1. Acid characteristics of samples.

Sample	Weak Acid Sites, μmol/g	Medium Acid Sites, μmol/g	Strong Acid Sites, μmol/g	Total, μmol/g
SiO_2 (RH)	11	15	52	78
3 wt.% CuO/SiO_2 (RH)	107	34	12	153
5 wt.% CuO/SiO_2 (RH)	121	6	34	161
SiO_2	400	-	82	482
3 wt.% CuO/SiO_2	802	-	46	848
5 wt.% CuO/SiO_2	934	-	34	968

3.2. Catalytic Performance for Non-Oxidation of Ethanol

SiO_2 (RH), SiO_2 carriers, and the synthesized catalysts 3–5 wt.% CuO/SiO_2 (RH), 3–5 wt.% CuO/SiO_2 were studied in the non-oxidative dehydrogenation of ethanol to acetaldehyde in the range of 150–400 °C with a volume rate of ethanol (WHSV) in the range of 0.5–1.5 h^{-1}. The results of comparative tests showed that among the copper-containing catalysts, the most efficient and selective in relation to acetaldehyde is the 3 wt.% CuO/SiO_2 (RH) catalyst. On this catalyst, the highest selectivity for acetaldehyde is 47% at 350 °C and an ethanol volumetric flow rate (WHSV) of 0.5 h^{-1}. A further increase in the reaction temperature to 400 °C leads to a decrease in the selectivity for acetaldehyde by 39% due to an increase in the concentration of ethanol decomposition products (CO, CO_2, CH_4, H_2) in the reaction products (Scheme 1).

Among the carriers, SiO_2 (RH) is effective, and the selectivity for acetaldehyde is 28%. For further discussion of the results obtained, we selected 3–5 wt.% CuO/SiO_2 and 3–5 wt.% CuO/ SiO_2 (RH).

The comparative results obtained at the most effective reaction temperature of 350 °C and an ethanol flow rate of 0.5 h^{-1} are shown in Table 2.

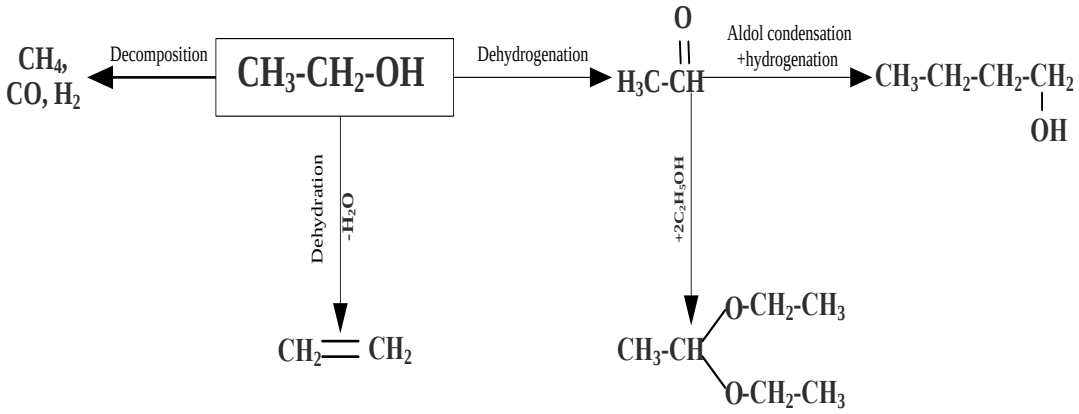

Scheme 1. Transformation of ethanol on CuO/SiO_2 (RH) catalyst.

Table 2. Conversion of ethanol and selectivity of reaction products at a reaction temperature of 350 °C, WHSV = 0.5 h^{-1}.

Samples	X_{EtOH}, %	C_2H_4, C_2H_6	AA	CH_4	CO	CO_2	H_2	H_2O	Other Products (Dietoxyethane, *n*-Butanol)
SiO_2	30	14	2	25	30	11	17	2	-
SiO_2 (RH)	42	0.3	28	13	12	10	30	4.3	2.0 (DEE), 0.4 (But)
3 wt.% CuO/SiO_2	63	6	22	13	22	10	25	2	-
3 wt.% CuO/SiO_2 (RH)	70	0.4	47	0.2	0.1	0.1	50	-	2.2 (DEE)
5 wt.% CuO/SiO_2	74	1	31	8	10	9	38	3	-
5 wt.% CuO/SiO_2 (RH)	85	-	42	0.2	0.2	0.1	51	-	5.5(DEE), 1(But)

The non-oxidative dehydrogenation of ethanol on SiO_2 and SiO_2 (RH) carriers leads to the formation of ethylene, acetaldehyde, and gas products such as methane, carbon oxides, and hydrogen, due to the reaction of the dehydration, dehydration, and decomposition of ethanol, respectively [60–62] (Scheme 1).

On SiO_2 (RH), in addition to the above reactions, ethanol reacts with acetaldehyde to diethoxyethane. Acetaldehyde is further deformed to form butanol [12,63]. The support of copper oxide on the SiO_2 and SiO_2 (RH) carriers leads to an increase in the selectivity of the dehydrogenation reaction to acetaldehyde and hydrogen, which indicates that copper oxide is an active site for ethanol dehydrogenation. The activity of the samples in ethanol conversion increases symbatically with an increase in the total acidity of the samples. The activity and selectivity of the 3 wt.% CuO/SiO_2 (RH) catalyst in the non-oxidative dehydrogenation of ethanol to acetaldehyde is higher than that of 3 wt.% CuO/SiO_2, which may be associated with an increase in the dispersion of active sites and the existence of medium acid sites; the data are consistent with the results of SEM, TPR-H_2, and TPD-NH_3. Ethanol conversion and acetaldehyde selectivity increase with rising copper oxide content on the carrier, regardless of the nature of the support. According to the literature [15,16], when ethanol is dehydrogenated, an equimolar amount of acetaldehyde and hydrogen is formed. However, in our case, the number of acetaldehyde formed is less than the amount of hydrogen. It has to do with the fact that gas reaction products such as methane and carbon oxides are formed not only as a result of the decomposition of ethanol but also from acetaldehyde. In the case of SiO_2 (RH) and 3 wt.% CuO/SiO_2 (RH), acetaldehyde is deformed before diethoxyethane and butanol.

The highest selectivity for acetaldehyde is observed on a catalyst of 3 wt.% CuO/SiO_2 (RH), which has the largest number of medium acid sites. On the catalyst 3 wt.% CuO/SiO_2 (RH), the selectivity for acetaldehyde is 47%, which is relatively higher compared to

the known catalysts Cu/ZrO_2 (S_{AA} = 21%) [27], Cu/Al_2O_3 (S_{AA} = 32%) [25], Cu/C (S_{AA} = 15%) [64], and Ni/SiO_2 (S_{AA} = 1.7%) [65].

According to [12], medium acid sites relate to ammonia adsorbed on strongly acid Lewis sites. Therefore, the existence of strongly acidic Lewis sites has a positive effect on the selectivity of the catalyst for acetaldehyde.

4. Conclusions

In this work, efficient low-percentage catalysts based on copper oxide were established using silicon dioxide SiO_2 (RH) as a carrier, synthesized from a renewable raw material—rice husk—to produce acetaldehyde. The synthesized catalysts were first studied in the non-oxidative dehydrogenation of ethanol. According to FTIR and XRD data, the hydrophilicity and hydrophobicity of silicon oxide play a major role in the preparation of catalysts. SiO_2 (RH) is more hydrophobic compared to SiO_2, which allowed copper oxide to concentrate on its surface in the form of a "crust", which is very important in the synthesis of low-percentage catalysts. Due to this, the active sites are more available for interaction with the molecules of the reactants. According to SEM, XRD, and TPR-H_2, the use of SiO_2 (RH) as a carrier leads to an increase in the dispersion of copper oxide particles, which is an active site for ethanol dehydrogenation. The results of TPD-ammonia showed that the support of copper oxide on the SiO_2 and SiO_2 (RH) carriers lead to an increase in the total acidity of the samples. Compared to SiO_2 and 3 wt.% CuO/SiO_2, SiO_2 (RH), and 3 wt.% CuO/SiO_2 (RH) have medium acid sites in addition to weak and strong acid sites. It can be assumed that the activity of low-percentage copper-containing catalysts in the non-oxidative dehydrogenation of ethanol symbatically increases with the rise in the total acidity of the samples, while the selectivity for acetaldehyde depends on the presence of medium acid sites. The highest acetaldehyde selectivity of 47% is observed on the 3 wt.% CuO/SiO_2 (RH) catalyst, which has the highest number of medium acid sites.

It follows from the results of the FTIR analysis that silicon oxide obtained from rice husks is stable to the effects of the reaction medium, that is, it does not change its structure compared to synthetic silicon oxide. The obtained results show that copper catalysts supported by silicon oxide from rice husks have good characteristics for the non-oxidative dehydrogenation of ethanol into valuable products.

Author Contributions: Conceptualization, G.Y. and K.D.; methodology, S.A., M.A. and K.A.; software, K.B. and B.B.; validation, K.D., G.Y. and M.M.; formal analysis, M.A. and K.A.; investigation, G.Y., M.M., S.A. and K.A.; resources, M.A., B.B. and S.A.; data curation, K.D.; writing—original draft preparation, G.Y., M.M. and K.A.; writing—review and editing, G.Y., M.M. and K.D.; visualization, S.A. and K.B.; supervision, K.D. and G.Y.; project administration, G.Y. All authors have read and agreed to the published version of the manuscript.

Funding: The work was carried out within the framework of the project of the Ministry of Education and Science of the Republic of Kazakhstan «Scientific aspects of the creation of composite materials with specified catalytic properties for the synthesis of acetaldehyde from renewable raw materials—bioethanol» (Grant No. AP08855936).

Institutional Review Board Statement: Not applicable.

Informed Consent Statement: Not applicable.

Data Availability Statement: Not applicable.

Conflicts of Interest: The authors declare no conflict of interest.

References

1. Caro, C.; Thirunavukkarasu, K.; Anilkumar, M.; Shiju, N.R.; Rothenberg, G. Selective Autooxidation of Ethanol over Titania-Supported Molybdenum Oxide Catalysts: Structure and Reactivity. *Adv. Synth. Catal.* **2012**, *354*, 1327–1336. [CrossRef]
2. Zhang, H.; Tan, H.R.; Jaenicke, S.; Chuah, G.K. Highly efficient and robust Cu catalyst for non-oxidative dehydrogenation of ethanol to acetaldehyde and hydrogen. *J. Catal.* **2020**, *389*, 19–28. [CrossRef]

3. Takei, T.; Iguchi, N.; Haruta, M. Synthesis of Acetoaldehyde, Acetic Acid, and Others by the Dehydrogenation and Oxidation of Ethanol. *Catal. Surv. Asia* **2011**, *15*, 80–88. [CrossRef]
4. Xu, J.; Xu, X.C.; Yang, X.J.; Han, Y.F. Silver/hydroxyapatite foam as a highly selective catalyst for acetaldehyde production via ethanol oxidation. *Catal. Today* **2016**, *276*, 19–27. [CrossRef]
5. Tang, C.; Zhai, Z.; Li, X.; Sun, L.; Bai, W. Sustainable production of acetaldehyde from lactic acid over the magnesium aluminate spinel. *J. Taiwan Inst. Chem. Eng.* **2016**, *58*, 97–106. [CrossRef]
6. Liu, P.; Hensen, E.J.M. Highly Efficient and Robust Au/$MgCuCr_2O_4$ Catalyst for Gas-Phase Oxidation of Ethanol to Acetaldehyde. *J. Am. Chem. Soc.* **2013**, *135*, 14032–14035. [CrossRef]
7. Santacesaria, E.; Carotenuto, G.; Tesser, R.; Di Serio, M. Ethanol Dehydrogenation to Ethyl Acetate by Using Copper and Copper Chromite Catalysts. *Chem. Eng. J.* **2012**, *179*, 209–220. [CrossRef]
8. Dossumov, K.; Yergazieva, G.Y.; Churina, D.H.; Tayrabekova, S.Z.; Tulebayev, E.M. Effect of the Method of Preparation of a Supported Cerium Oxide Catalyst on Its Activity in the Conversion of Ethanol to Ethylene. *Theor. Exp. Chem.* **2016**, *52*, 123–126. [CrossRef]
9. Dosumov, K.; Ergazieva, G.E.; Churina, D.K.; Tel'baeva, M.M. Cerium-Containing Catalysts for Converting Ethanol into Ethylene. *Russ. J. Phys. Chem. A* **2014**, *88*, 1806–1808. [CrossRef]
10. Galbe, M.; Zacchi, G. A Review of the Production of Ethanol from Softwood. *Appl. Microbiol. Biotechnol.* **2002**, *59*, 618–628. [CrossRef]
11. Sun, Y.; Cheng, J. Hydrolysis of Lignocellulosic Materials for Ethanol Production: A Review. *Bioresour. Technol.* **2002**, *83*, 1–11. [CrossRef]
12. Yergaziyeva, G.Y.; Dossumov, K.; Mambetova, M.M.; Strizhak, P.Y.; Kurokawa, H.; Baizhomartov, B. Effect of Ni, La, and Ce Oxides on a Cu/Al_2O_3 Catalyst with Low Copper Loading for Ethanol Non-oxidative Dehydrogenation. *Chem. Eng. Technol.* **2021**, *44*, 1890–1899. [CrossRef]
13. Pinthong, P.; Praserthdam, P.; Jongsomjit, B. Oxidative Dehydrogenation of Ethanol over Vanadium- and Molybdenum-Modified Mg-Al Mixed Oxide Derived from Hydrotalcite. *J. Oleo Sci.* **2019**, *68*, 679–687. [CrossRef] [PubMed]
14. Sushkevich, V.L.; Ivanova, I.I.; Taarning, E. Mechanistic Study of Ethanol Dehydrogenation over Silica-Supported Silver. *ChemCatChem* **2013**, *5*, 2367–2373. [CrossRef]
15. Amandusson, H.; Ekedahl, L.-G.; Dannetun, H. Isotopic Study of Ethanol Dehydrogenation over a Palladium Membrane. *J. Catal.* **2000**, *195*, 376–382. [CrossRef]
16. Liang, Y.Q.; Cui, Z.D.; Zhu, S.L.; Liu, Y.; Yang, X.J. Silver Nanoparticles Supported on TiO_2 Nanotubes as Active Catalysts for Ethanol Oxidation. *J. Catal.* **2011**, *278*, 276–287. [CrossRef]
17. Yu, D.; Dai, W.; Wu, G.; Guan, N.; Li, L. Stabilizing copper species using zeolite for ethanol catalytic dehydrogenation to acetaldehyde. *Chin. J. Catal.* **2019**, *9*, 1375–1384. [CrossRef]
18. Tonner, S.P.; Trimm, D.L.; Wainwright, M.S.; Cant, N.W. Dehydrogenation of Methanol to Methyl Formate over Copper Catalysts. *Ind. Eng. Chem. Prod. Res. Dev.* **1984**, *23*, 384–388. [CrossRef]
19. Guan, Y.; Hensen, E.J.M. Ethanol Dehydrogenation by Gold Catalysts: The Effect of the Gold Particle Size and the Presence of Oxygen. *Appl. Catal. Gen.* **2009**, *361*, 49–56. [CrossRef]
20. Sitthisa, S.; Resasco, D.E. Hydrodeoxygenation of Furfural Over Supported Metal Catalysts: A Comparative Study of Cu, Pd and Ni. *Catal. Lett.* **2011**, *141*, 784–791. [CrossRef]
21. Tu, Y.J.; Chen, Y.-W. Effects of Alkaline-Earth Oxide Additives on Silica-Supported Copper Catalysts in Ethanol Dehydrogenation. *Ind. Eng. Chem. Res.* **1998**, *37*, 2618–2622. [CrossRef]
22. Tu, Y.J.; Chen, Y.-W. Effects of Alkali Metal Oxide Additives on Cu/SiO_2 Catalyst in the Dehydrogenation of Ethanol. *Ind. Eng. Chem. Res.* **2001**, *40*, 5889–5893. [CrossRef]
23. Wang, C.; Garbarino, G.; Allard, L.F.; Wilson, F.; Busca, G.; Flytzani-Stephanopoulos, M. Low-Temperature Dehydrogenation of Ethanol on Atomically Dispersed Gold Supported on $ZnZrO_x$. *ACS Catal.* **2016**, *6*, 210–218. [CrossRef]
24. Shan, J.; Janvelyan, N.; Li, H.; Liu, J.; Egle, T.M.; Ye, J.; Biener, M.M.; Biener, J.; Friend, C.M.; Flytzani-Stephanopoulos, M. Selective Non-Oxidative Dehydrogenation of Ethanol to Acetaldehyde and Hydrogen on Highly Dilute NiCu Alloys. *Appl. Catal. B Environ.* **2017**, *205*, 541–550. [CrossRef]
25. Tayrabekova, S.; Mäki-Arvela, P.; Peurla, M.; Paturi, P.; Eränen, K.; Ergazieva, G.E.; Aho, A.; Murzin, D.Y.; Dossumov, K. Catalytic Dehydrogenation of Ethanol into Acetaldehyde and Isobutanol Using Mono- and Multicomponent Copper Catalysts. *C. R. Chim.* **2018**, *21*, 194–209. [CrossRef]
26. Witzke, M.E.; Dietrich, J.P.; Ibrahim, M.Y.S.; Al-Bardan, K.; Triezenberg, M.D.; Flaherty, D.W. Spectroscopic evidence for origins of size and support effects on selectivity of Cu nanoparticle dehydrogenation catalysts. *Chem. Commun.* **2017**, *53*, 597–600. [CrossRef]
27. Freitas, I.C.; Damyanova, S.; Oliveira, D.C.; Marques, C.M.P.; Bueno, J.M.C. Effect of Cu Content on the Surface and Catalytic Properties of Cu/ZrO_2 Catalyst for Ethanol Dehydrogenation. *J. Mol. Catal. Chem.* **2014**, *381*, 26–37. [CrossRef]
28. Cassinelli, W.H.; Martins, L.; Passos, A.R.; Pulcinelli, S.H.; Rochet, A.; Briois, V.; Santilli, C.V. Correlation between Structural and Catalytic Properties of Copper Supported on Porous Alumina for the Ethanol Dehydrogenation Reaction. *ChemCatChem* **2015**, *7*, 1668–1677. [CrossRef]
29. Cassinelli, W.H.; Martins, L.; Magnani, M.; Pulcinelli, S.H.; Briois, V.; Santilli, C.V. Time-Resolved XAS/MS/Raman Monitoring of Mutual Copper Self-Reduction and Ethanol Dehydrogenation Reactions. *RSC Adv.* **2016**, *6*, 20453–20457. [CrossRef]

30. Rossetti, I.; Biffi, C.; Bianchi, C.L.; Nichele, V.; Signoretto, M.; Menegazzo, F.; Finocchio, E.; Ramis, G.; Di Michele, A. Ni/SiO_2 and Ni/ZrO_2 Catalysts for the Steam Reforming of Ethanol. *Appl. Catal. B Environ.* **2012**, *117–118*, 384–396. [CrossRef]
31. Ohira, M.; Liu, H.; He, D.; Hirata, Y.; Sano, M.; Suzuki, T.; Miyake, T. Catalytic Performance and Reaction Pathways of Cu/SiO_2 and ZnO/SiO_2 for Dehydrogenation of Ethanol to Acetaldehyde. *J. Jpn. Pet. Inst.* **2018**, *61*, 205–212. [CrossRef]
32. He, X.; Liu, H. Efficient Synthesis of 1,1-Diethoxyethane via Sequential Ethanol Reactions on Silica-Supported Copper and H-Y Zeolite Catalysts. *Catal. Today* **2014**, *233*, 133–139. [CrossRef]
33. Wang, Q.-N.; Shi, L.; Lu, A.-H. Highly Selective Copper Catalyst Supported on Mesoporous Carbon for the Dehydrogenation of Ethanol to Acetaldehyde. *ChemCatChem* **2015**, *7*, 2846–2852. [CrossRef]
34. Li, M.; Lu, W.; He, L.; Schüth, F.; Lu, A. Tailoring the Surface Structure of Silicon Carbide Support for Copper Catalyzed Ethanol Dehydrogenation. *ChemCatChem* **2019**, *11*, 481–487. [CrossRef]
35. Wang, Q.N.; Shi, L.; Li, W.; Li, W.C.; Si, R.; Schüth, F.; Lu, A.H. Cu supported on thin carbon layer-coated porous SiO_2 for efficient ethanol dehydrogenation. *Catal. Sci. Technol.* **2018**, *8*, 472–479. [CrossRef]
36. Shukla, S.S.; Chava, R.; Appari, S.; Bahurudeen, A.; Kuncharam, B.V.R. Sustainable use of rice husk for the cleaner production of value-added products. *J. Environ. Chem. Eng.* **2022**, *10*, 106899. [CrossRef]
37. Materazzi, M.; Foscolo, P.U. The role of waste and renewable gas to decarbonize the energy sector. In *Substitute Natural Gas from Waste: Technical Assessment and Industrial Applications of Biochemical and Thermochemical Processes*; Elsevier: Amsterdam, The Netherlands, 2019; pp. 1–19. [CrossRef]
38. Ang, T.N.; Ngoh, G.C.; Chua, A.S.M.; Lee, M.G. Elucidation of the effect of ionic liquid pretreatment on rice husk via structural analyses. *Biotechnol. Biofuels* **2012**, *5*, 67. [CrossRef]
39. Materazzi, M. Gasification of Waste Derived Fuels in Fluidized Beds: Fundamental Aspects and Industrial Challenges. In *Clean Energy from Wast*; Springer: Cham, Switzerland, 2017; pp. 19–63. [CrossRef]
40. Shah, S.A.; Soomar, M.; Hussain, A. Comparative emission analysis of bituminous coal, Sugarcane Bagasse and Rice Husk. *Sind. Univ. Res. J.* **2016**, *48*, 685–688.
41. Azat, S.; Sartova, Z.; Bekseitova, K.; Askaruly, K. Extraction of high-purity silica from rice husk via hydrochloric acid leach-ingtreatment. *Turk. J. Chem.* **2019**, *43*, 1258–1269. [CrossRef]
42. Myachina, M.; Gavrilova, N.; Nazarov, V. Formation of Molybdenum Blue Nanoparticles in the Organic Reducing Area. *Molecules* **2021**, *26*, 4438. [CrossRef]
43. Llez, L.T.E.; Rubio, J.; Rubio, F.; Morales, E.; Oteo, J.L. Synthesis of Inorganic-Organic Hybrid Materials from TEOS, TBT and PDMS. *J. Mater. Sci.* **2003**, *38*, 1773–1780.
44. Bakdash, R.S.; Aljundi, I.H.; Basheer, C.; Abdulazeez, I. Rice Husk Derived Aminated Silica for the Efficient Adsorption of Different Gases. *Sci. Rep.* **2020**, *10*, 19526. [CrossRef] [PubMed]
45. Chang, F.-W.; Yang, H.-C.; Roselin, L.S.; Kuo, W.-Y. Ethanol Dehydrogenation over Copper Catalysts on Rice Husk Ash Prepared by Ion Exchange. *Appl. Catal. Gen.* **2006**, *304*, 30–39. [CrossRef]
46. Yalçin, N.; Sevinç, V. Studies on Silica Obtained from Rice Husk. *Ceram. Int.* **2001**, *27*, 219–224. [CrossRef]
47. Guerreiro, E.D.; Gorriz, O.F.; Rivarola, J.B.; Arrúa, L.A. Characterization of Cu/SiO_2 Catalysts Prepared by Ion Exchange for Methanol Dehydrogenation. *Appl. Catal. Gen.* **1997**, *165*, 259–271. [CrossRef]
48. Baltes, C.; Vukojevic, S.; Schuth, F. Correlations between Synthesis, Precursor, and Catalyst Structure and Activity of a Large Set of CuO/ZnO/Al_2O_3 Catalysts for Methanol Synthesis. *J. Catal.* **2008**, *258*, 334–344. [CrossRef]
49. Águila, G.; Gracia, F.; Cortés, J.; Araya, P. Effect of Copper Species and the Presence of Reaction Products on the Activity of Methane Oxidation on Supported CuO Catalysts. *Appl. Catal. B Environ.* **2008**, *77*, 325–338. [CrossRef]
50. Hao, X.-Y.; Zhang, Y.-Q.; Wang, J.-W.; Zhou, W.; Zhang, C.; Liu, S. A Novel Approach to Prepare MCM-41 Supported CuO Catalyst with High Metal Loading and Dispersion. *Microporous Mesoporous Mater.* **2006**, *88*, 38–47. [CrossRef]
51. Ding, J.; Popa, T.; Tang, J.; Gasema, K.A.M.; Fan, M.; Zhong, Q. Highly selective and stable Cu/SiO_2 catalysts prepared with a green method for hydrogenation of diethyl oxalate into ethylene glycol. *Appl. Catal. B Environ.* **2017**, *209*, 530. [CrossRef]
52. Dossumov, K.; Ergazieva, G.E.; Ermagambet, B.T.; Telbayeva, M.M.; Mambetova, M.M.; Myltykbayeva, L.K.; Kassenova, Z.M. Role of Ceria in Several Energy-Related Catalytic Transformations. *Chem. Pap.* **2020**, *74*, 373–388. [CrossRef]
53. Dossumov, K.; Ergazieva, G.E.; Ermagambet, B.T.; Myltykbaeva, L.K.; Telbaeva, M.M.; Mironenko, A.V.; Mambetova, M.M.; Kassenova, Z. Morphology and Catalytic Properties of Cobalt-Containing Catalysts Synthesized by Different Means. *Russ. J. Phys. Chem. A* **2020**, *94*, 880–882. [CrossRef]
54. Cavuoto, D.; Zaccheria, A.; Ravasio, N. Some Critical Insights into the Synthesis and Applications of Hydrophobic Solid Catalysts. *J. Catal.* **2020**, *10*, 1337. [CrossRef]
55. Selva Roselin, L.; Chiu, H.-W. Production of hydrogen by oxidative steam reforming of methanol over Cu/SiO_2 catalysts. *J. Saudi Chem. Soc.* **2018**, *22*, 692. [CrossRef]
56. Xi, X.; Ma, S.; Chen, J.-F.; Zhang, Y. Promotional Effects of Ce, Mn and Fe Oxides on CuO/SiO_2 Catalysts for CO Oxidation. *J. Environ. Chem. Eng.* **2014**, *2*, 1011–1017. [CrossRef]
57. Liu, Z.; Amiridis, M.D.; Chen, Y. Characterization of CuO Supported on Tetragonal ZrO_2 Catalysts for N_2 O Decomposition to N_2. *J. Phys. Chem. B* **2005**, *109*, 1251–1255. [CrossRef]
58. Van Der Grift, C.J.G.; Wielers, A.F.H.; Mulder, A.; Geus, J.W. The reduction behaviour of silica-supported copper catalysts prepared by deposition-precipitation. *Thermochim. Acta* **1990**, *171*, 95–113. [CrossRef]

59. Zhang, J.; Chen, T.; Jiao, Y.; Cheng, M.; Wang, L.-L.; Wang, J.-L.; Li, X.-Y.; Chen, Y.-Q. Improved Activity of Ni–Mo/SiO_2 Bimetallic Catalyst Synthesized via Sol-Gel Method for Methylcyclohexane Cracking. *Pet. Sci.* **2021**, *18*, 1530–1542. [CrossRef]
60. Pang, J.; Zheng, M.; He, L.; Li, L.; Pan, X.; Wang, A.; Wang, X.; Zhang, T. Upgrading Ethanol to N-Butanol over Highly Dispersed Ni–MgAlO Catalysts. *J. Catal.* **2016**, *344*, 184–193. [CrossRef]
61. Benito, P.; Vaccari, A.; Antonetti, C.; Licursi, D.; Schiarioli, N.; Rodriguez-Castellón, E.; Raspolli Galletti, A.M. Tunable Copper-Hydrotalcite Derived Mixed Oxides for Sustainable Ethanol Condensation to n-Butanol in Liquid Phase. *J. Clean. Prod.* **2019**, *209*, 1614–1623. [CrossRef]
62. Larina, O.V.; Valihura, K.V.; Kyriienko, P.I.; Vlasenko, N.V.; Balakin, D.Y.; Khalakhan, I.; Čendak, T.; Soloviev, S.O.; Orlyk, S.M. Successive Vapour Phase Guerbet Condensation of Ethanol and 1-Butanol over Mg-Al Oxide Catalysts in a Flow Reactor. *Appl. Catal. Gen.* **2019**, *588*, 117265. [CrossRef]
63. Rechi Siqueira, M.; Micali Perrone, O.; Metzker, G.; de Oliveira Lisboa, D.C.; Thoméo, J.C.; Boscolo, M. Highly Selective 1-Butanol Obtained from Ethanol Catalyzed by Mixed Metal Oxides: Reaction Optimization and Catalyst Structure Behavior. *Mol. Catal.* **2019**, *476*, 110516. [CrossRef]
64. Ob-eye, J.; Praserthdam, P.; Jongsomjit, B. Dehydrogenation of Ethanol to Acetaldehyde over Different Metals Supported on Carbon Catalysts. *J. Catal.* **2019**, *9*, 66. [CrossRef]
65. Calles, J.; Carrero, A.; Vizcaíno, A.; Lindo, M. Effect of Ce and Zr Addition to Ni/SiO_2 Catalysts for Hydrogen Production through Ethanol Steam Reforming. *J. Catal.* **2015**, *5*, 58–76. [CrossRef]